Post-Print

This is the accepted version of:

D. Vimercati, A. Kluwick, A. Guardone
Oblique Waves in Steady Supersonic Flows of Bethe-Zel'dovich-Thompson Fluids
Journal of Fluid Mechanics, Vol. 855, 2018, p. 445-468
doi:10.1017/jfm.2018.633

Oblique waves in steady supersonic flows of Bethe-Zel'dovich-Thompson fluids

Davide Vimercati[1], Alfred Kluwick[2], Alberto Guardone[1,]†

Department of Aerospace Science and Technology, Politecnico di Milano
Via La Masa 34, 20156 Milano, Italy

Institute of Fluid Mechanics and Heat Transfer, Vienna University of Technology
Getreidemarkt 9, 1060 Vienna, Austria

(Received xx; revised xx; accepted xx)

Steady self-similar solutions to the supersonic flow of Bethe-Zel'dovich-Thompson fluids past compressive and rarefactive ramps are derived. Inviscid, non-heat-conducting, non-reacting and single-phase vapour or gas flow is assumed. For convex isentropes and shock adiabats in the pressure–specific volume plane (classical gasdynamic regime), the well-known oblique shock and centred Prandtl-Meyer fan occur at a compressive and rarefactive ramp, respectively. For non-convex isentropes and shock adiabats (non-classical gasdynamic regime), four additional wave configurations may possibly occur; these are composite waves in which a Prandtl-Meyer fan is adjacent up to two oblique shock waves. The steady two-dimensional counterparts of the wave curves defined for the one-dimensional Riemann problem are constructed. In the present context, such curves consist of all the possible states connected to a given initial state (namely, the uniform state upstream of the ramp/wedge) by means of a steady self-similar solution. In addition to the classical case, as many as six non-classical wave curve configurations are singled out. Moreover, the necessary conditions leading to each type of wave curves are analysed and a map of the upstream states leading to each configuration is determined.

1. Introduction

In the supersonic ramp problem, a supersonic uniform stream is deflected onto a sharp corner. The steady-state solution configurations of the ramp problem are fundamental in gasdynamics, as they provide global or local structures in diverse flow fields: supersonic intakes and discharges, turbine flows, steady regular and Mach reflections, two-dimensional Riemann problems, just to mention a few. In the classical theory of gasdynamics, a compressive ramp produces two possible steady state configurations — the weak and the strong oblique shock configurations — provided the wedge angle doesn't exceed the detachment angle, whereas a rarefaction ramp gives rise to a centred Prandtl-Meyer fan, see e.g. Thompson 1988. The picture given here applies to all substances described by convex equations of state (EoS), namely those featuring positive curvature of the isentropes in the pressure–specific volume diagram or, in non-dimensional terms, those exhibiting positive values of the fundamental derivative of gasdynamics Γ,

$$\Gamma = \frac{v^3}{2c^2}\left(\frac{\partial^2 P}{\partial v^2}\right)_s = 1 - \frac{v}{c}\left(\frac{\partial c}{\partial v}\right)_s, \tag{1.1}$$

where P is the pressure, v the specific volume, s the specific entropy and c the speed of sound. The thermodynamic quantity Γ was introduced by Thompson (1971), due to

† Email address for correspondence: alberto.guardone@polimi.it

the paramount role that it plays in delineating the dynamic behaviour of compressible flows (Bethe 1942; Zel'dovich 1946; Thompson & Lambrakis 1973; Landau & Lifshitz 1987). Note, in particular, that $1-\Gamma$ is a non-dimensional measure of the sound-speed variation with the density along isentropic processes. The asymptotic conditions on the EoS stemming from physical requirements imply that Γ is positive in the dilute-gas limit. Indeed, for a perfect gas the fundamental derivative is given by $\Gamma=(\gamma+1)/2>1$, where γ is the ratio of the specific heats. However, negative nonlinearities can in principle be observed in the close proximity to the liquid-vapour saturation curve and critical point. In substances conforming to a 3-dimensional Ising-like systems (including, e.g., common fluids such as water, methane, carbon dioxide), negative nonlinearity is predicted to appear in the near-critical vapour-liquid equilibrium region due to critical-point effects (Nannan *et al.* 2014, 2016). In addition, a family of high molecularly complex fluids, commonly referred to as Bethe-Zel'dovich-Thompson (BZT) fluids, is expected to exhibit negative nonlinearity in a finite vapour-phase thermodynamic region neighbouring the saturation curve. According to modern and most accurate thermodynamic models, candidate BZT fluids are believed to belong to the classes of hydrocarbons, fluorocarbons and siloxanes (Lambrakis & Thompson 1972; Cramer 1989*a*; Colonna *et al.* 2007). In spite of the various attempts (Ivanov & Novikov 1961; Borisov *et al.* 1983; Kutateladze *et al.* 1987; Fergason *et al.* 2001; Thompson *et al.* 1986; Fergason *et al.* 2003; Colonna *et al.* 2008; Mathijssen *et al.* 2015), experimental evidence of non-classical behaviour is lacking due to many technical problems, e.g. the risk of explosion and thermal decomposition at the high temperatures where non-classical effects would potentially occur and the very limited pressure and temperature ranges encompassing the negative-Γ region predicted by state-of-the-art thermodynamic models.

In the thermodynamic domain where the fundamental derivative can possibly change its sign, the EoS is locally non-convex. Local loss of convexity has dramatic implications on the governing equations, as it possibly leads to the formation of non-classical waves such as expansion shocks, shock waves with either upstream or downstream sonic states, composite and split waves (Thompson 1971; Thompson & Lambrakis 1973; Cramer & Kluwick 1984; Cramer & Sen 1986, 1987; Cramer 1989*b*; Menikoff & Plohr 1989; Bates & Montgomery 1999; Kluwick 2001).

Our understanding of the basic mechanisms and flow structures in non-classical gas-dynamics mainly originates from the investigation of unsteady one-dimensional flows (see, e.g., Cramer & Kluwick 1984; Cramer & Sen 1986) and steady nozzle flows (see Cramer & Fry 1993; Kluwick 1993; Guardone & Vimercati 2016). Within the non-classical context, the steady supersonic flow past solid wedges was only partially examined in the scientific literature. In his pioneering work, Thompson (1971) studied the formation of the two elementary wave configurations in the ramp problem for negative-Γ fluids: the oblique rarefaction shock and the compressive Prandtl-Meyer fan, which represent the non-classical counterparts of the classical compression shock and rarefaction fan. Recently, the ramp problem for BZT fluids was investigated by Kluwick & Cox (2018) in the transonic approximation, with the further assumption that $|\Gamma|\ll 1$, namely in the vicinity of the transition line $\Gamma=0$. In this framework, the parameter space determining the solution configuration includes the wedge angle, the upstream Mach number, the upstream fundamental derivative and its isentropic derivative with respect to the density. The authors showed that, through the scaling originally introduced by Cramer & Tarkenton (1992), the parameter space can be reduced to dimension two. Five different ranges of these similarities parameters were identified, which correspond to qualitative different flow scenarios. The resulting picture is considerably rich, due to the possibility of observing, in addition to inverted gasdynamic behaviour (viz.

rarefaction oblique shocks and compression Prandtl-Meyer fans), also composite waves configurations, in which a Prandtl-Meyer fan is adjacent to an oblique shock wave.

Menikoff & Plohr (1989) suggested the possibility of studying planar, supersonic and self-similar flows moving from the one-dimensional Riemann problem for an arbitrary equation of state. If a solution exhibiting no length scale is sought (e.g. self-similar solutions), a set of ordinary differential equations is obtained which produces three distinct waves families, for both two-dimensional steady supersonic flows and unsteady one-dimensional flows (see, e.g., Godlewski & Raviart 2013). One wave family is linearly degenerate (in two dimensions with a multiplicity of two) and corresponds to contact discontinuities, while the other two families are non-degenerate (except at isolated points in non-classical flows) and are associated with acoustic and shock waves. Oblique shocks in two dimensions satisfy the one-dimensional Rankine-Hugoniot relations in the direction normal to the shock front. Smooth solutions consist of wave fans, spreading either in the two-dimensional space or in one dimension as time progresses. Thus, unsteady normal shocks translate into steady oblique shocks and unsteady wave fans become Prandtl-Mayer waves. The qualitative equivalence between these wave patterns is key to extend the tools and concept developed for the one-dimensional Riemann problem to steady, self-similar flow in two dimensions.

In this study, the steady supersonic planar flow of BZT fluids over compressive and rarefactive ramps is systematically investigated by identifying each self-similar flow configuration that is compatible with the boundary condition imposed by the solid wedge. Following the same line of Menikoff & Plohr (1989), the analysis of the ramp problem is traced back to the construction of steady two-dimensional wave curves, which consist of all the states connected to a given supersonic upstream state by means of a steady self-similar planar wave. Similarities and differences with the wave curves of the one-dimensional Riemann problem are discussed. The proposed analytical approach — undertaken here in a fully non-linear perspective, differently from the asymptotic theory developed by Kluwick & Cox (2018) — leads to the identification of seven different wave-curve types, six of which are of purely non-classical type. The latter cases all include branches where the solution of the ramp problem consists of a composite wave (e.g. combination of Prandtl-Meyer fan and oblique shock). As the wave-curve configuration is determined by the properties of the uniform supersonic state upstream of the wedge, the corresponding parameter space (e.g. the upstream pressure, density and Mach number) is explored. Eventually, the necessary conditions for the occurrence of each of the identified wave-curve types are singled out and a map of the upstream states leading the different configurations is delineated.

The structure of this work is as follows. In §2, the mathematical description of the fluid flow is recalled for the special case of two-dimensional steady self-similar flows that are compatible with a prescribed supersonic conditions at upstream infinity. The elementary waves that can possibly occur in these flows are defined. In §3, we describe how the established concepts for the one-dimensional Riemann problem can be suitably translated into the present two-dimensional steady context, thus leading to the definition of the wave curves for the ramp problem. The construction of these curves from one-parameter families of elementary waves is treated. The structure of the wave curves is then analysed by first considering their projection in a thermodynamic plane (§4) and secondly those on common polar diagrams (§5). The van der Waals model of a BZT fluid is used for explanatory purposes. Section 6 presents the development of the map of the upstream states that are associated to each type of wave curve. Section 7 outlines the concluding remarks.

2. Formulation

We restrict our attention to the steady two-dimensional flow equations that model equilibrium fluid dynamics in the limit of vanishing viscosity and heat conductivity, namely steady two-dimensional Euler equations

$$\partial_x F_x(q) + \partial_y F_y(q) = 0, \tag{2.1}$$

where

$$q = (\rho, \rho u_x, \rho u_y, \rho e + \rho u^2/2) \tag{2.2}$$

is the vector of conservative variables, in which ρ is the density, u_x, u_y and u are the velocity x-component, y-component and magnitude, respectively, and e is the specific internal energy. The fluxes F_x and F_y are given by

$$F_x(q) = (\rho u_x, \rho u_x^2 + P, \rho u_x u_y, \rho h^t u_x), \tag{2.3}$$

$$F_y(q) = (\rho u_y, \rho u_x u_y, \rho u_y^2 + P, \rho h^t u_y), \tag{2.4}$$

where P is the pressure and $h^t = e + P/\rho + u^2/2$ is the specific total enthalpy.

The steady two-dimensional Euler equations are classified as elliptic, parabolic or hyperbolic depending on the value of the flow Mach number M,

$$M = u/c, \tag{2.5}$$

see, e.g., Godlewski & Raviart (2013). System (2.1) is of the elliptic type if $M < 1$ and of the parabolic type if $M = 1$. If $M > 1$, system (2.1) is hyperbolic in every direction (i.e. timelike direction) that is not perpendicular to characteristic lines (Dafermos 2010).

In a cartesian x–y coordinate system, we consider, with reference to the ramp problem, a solid boundary described by the the equations

$$y = 0, \qquad x \leqslant 0, \tag{2.6}$$

$$y = (\tan\vartheta_r)\, x, \qquad x > 0, \tag{2.7}$$

where ϑ_r is the ramp angle. The corner of the ramp is thus located at $x = 0$, $y = 0$. Along the solid wall, slip boundary condition is enforced. A uniform flow state is prescribed at infinite upstream $x = -\infty$, which is aligned with the wall ($u_y = 0$) and supersonic.

In this study, self-similar solutions of the steady supersonic ramp problem are examined. These are functions of the form $q(x, y) = w(y/x)$ that satisfy the integral form of the conservation law associated with (2.1) in the domain (circular sector) delimited by the solid wall, along with the boundary conditions imposed on the wall itself and at upstream infinity. On physical grounds, we shall also limit ourself to consider self-similar solutions that are piecewise C^1. Introducing $\xi = y/x$, this means that $w(\xi)$ is continuously differentiable except for a finite number of points at which w has a jump discontinuity or is continuous but not differentiable. As a consequence, we examine solutions that are constant along rays emanating from the corner of the ramp; in the solution flow field, a finite number of rays, carrying jump discontinuities in w or its gradient, separate circular sectors where w is continuously differentiable. In the following, the building blocks for the construction of self-similar solutions of the steady supersonic ramp problem are described. These are the continuously differentiable simple waves, the discontinuous waves (shocks and contacts) and the composite waves, which are combination of the previous ones.

2.1. *Simple waves*

The flow pattern corresponding to a non-trivial, continuously differentiable function $w(\xi)$ is called a centred simple wave and in the physical plane it takes the form of a fan, commonly denoted as Prandtl-Meyer fan, converging at a single point. At points where $w(\xi)$ is continuous and differentiable, equation (2.1) is equivalent to the generalized eigenvalue problem

$$\Big(A_y(w(\xi)) - \xi A_x(w(\xi))\Big)w'(\xi) = 0, \tag{2.8}$$

where $A_x(q) = D_q F_x(q)$ and $A_y(q) = D_q F_y(q)$ are the Jacobians of the fluxes. It follows that either $w'(\xi) = 0$ or

$$\xi = \lambda_k(w(\xi)), \qquad \text{for some } k \in \{1, ..., 4\} \tag{2.9}$$

and

$$w'(\xi) = r_k(w(\xi))/\alpha_k(w(\xi)), \qquad \text{for some } k \in \{1, ..., 4\}\,, \tag{2.10}$$

where λ_k and r_k denote the k-th eigenvalue and right eigenvector, respectively, in the generalized eigenvalue problem (2.8) and $\alpha_k = D_q\lambda_k(q)\cdot r_k(q)$ is the so-called nonlinearity factor (see appendix A). Note also that the ray marking the transition between a simple-wave region and a uniform flow region is a point of jump discontinuity for $w'(\xi)$.

Since $\xi = x/y$ is a real number, relation (2.9) implies that the eigenvalue λ_k is also real. It is well-known (see, e.g., Thompson 1988) that the characteristic equation of the eigenvalue problem (2.8) always gives a real root $\lambda = \tan\vartheta$ of multiplicity two, where $\vartheta = \tan^{-1}(u_y/u_x)$ is the angle formed by the particle path with the x-axis (positive if counter-clockwise), whereas the remaining roots are real if and only if the flow is supersonic ($M > 1$). For supersonic flow, the eigenvalues of the steady planar Euler equations can be written as

$$\lambda_1 = \tan(\vartheta - \mu), \quad \lambda_{2,3} = \tan\vartheta, \quad \lambda_4 = \tan(\vartheta + \mu), \tag{2.11}$$

in which the angle $\mu = \sin^{-1}(1/M)$ is called the Mach angle. The characteristic curves, having slope $\mathrm{d}y/\mathrm{d}x = \lambda_k$ in the physical x–y plane, are thus the particle paths and the curves that locally form an angle $\pm\mu$ with the particle paths. Because of this, the characteristics of the 1–field and 4–field (the k–field is the characteristic field associated with λ_k and r_k) are also referred to as right-running and left-running acoustic waves, respectively. Equation (2.9) implies that the rays in a centred simple wave correspond to characteristic lines.

Relation (2.10) asserts that the states within a centred simple wave all lie along an integral curve of $r_k(q)$. However, in order that $w'(\xi)$ stays finite, the nonlinearity factor appearing in (2.10) must not be zero. With a proper scaling of the eigenvectors, the nonlinearity factors read (appendix A)

$$\alpha_{1,4} = \mathit{\Gamma}, \quad \alpha_{2,3} = 0, \tag{2.12}$$

thus showing, together with relation (2.10), that continuously differentiable waves are not possible in the 2–field and 3–field (which are linearly degenerate and give rise to contact discontinuities, see §2.2) and in the 1–field and 4–field at degenerate points $\mathit{\Gamma} = 0$. In other words, centred simple waves can only take place in the acoustic wave families (1–field or 4–field) if $\mathit{\Gamma} \neq 0$.

For each characteristic field of an n-dimensional system of conservation laws (in our case $n = 4$) is defined a set of $n - 1$ Riemann invariants (Dafermos 2010). A Riemann invariant of the k-th field is a scalar-valued function that is constant along the integral curve of $r_k(q)$. The Riemann invariants of the 1–field and 4–field are the triplets

$$\begin{cases} s,\ h^t,\ \vartheta - \nu & \text{(1–field)}, \\ s,\ h^t,\ \vartheta + \nu & \text{(4–field)}, \end{cases} \tag{2.13}$$

where

$$\nu = \nu_0 + \int_{u_0}^{u} \sqrt{M^2-1}\frac{du}{u} = \nu_0 - \int_{P_0}^{P} \frac{\sqrt{M^2-1}}{\rho u^2} dP \tag{2.14}$$

is the Prandtl-Meyer function, in which subscript 0 refers to a reference state (in fluids exhibiting $\Gamma < 1$, the above forms of the Prandtl-Meyer function are valid at all velocities and pressures, contrarily to the more common form parametrized using the Mach number, see Cramer & Crickenberger 1992). Therefore, the flow field within a centred simple wave has constant entropy and total enthalpy. By examining the eigenvectors r_1 and r_4 (see appendix A), it is readily seen that $P'(\xi) \gtrless 0$, $u'(\xi) \lessgtr 0$ and $\vartheta'(\xi) \gtrless 0$ if $\Gamma \gtrless 0$ within left-running simple waves, while $P'(\xi) \lessgtr 0$, $u'(\xi) \gtrless 0$ and $\vartheta'(\xi) \gtrless 0$ if $\Gamma \gtrless 0$ in right-running simple waves.

2.2. *Shock waves and contact discontinuities*

The turning of a supersonic stream can also be accomplished by means of discontinuous waves. If w has a jump discontinuity along the ray ξ, the balance laws of mass, momentum and energy assume the form

$$[F_y - \xi F_x] = 0, \tag{2.15}$$

where $[\cdot]$ denotes the jump across the discontinuity. Equations (2.15) are the well-known set of Rankine-Hugoniot relations (see, e.g., Thompson 1988), which can be conveniently recast as

$$[\rho u_n] = 0, \tag{2.16}$$

$$[P + \rho u_n^2] = 0, \tag{2.17}$$

$$[\rho u_n u_t] = 0, \tag{2.18}$$

$$[\rho u_n h^t] = 0, \tag{2.19}$$

where u_n and u_t are the normal and tangential velocity components, with respect to the shock front. System (2.16)-(2.19) includes both contact discontinuities and shock waves, which are distinguished according to the value of the mass flux $m = \rho u_n$ across the discontinuity front. For contact discontinuities $m = 0$, while for shock waves $m \neq 0$.

The states that can be connected by means of contact discontinuities lie on the integral curves of $r_2(q)$ and $r_3(q)$, see Godlewski & Raviart (2013). The corresponding Riemann invariants are

$$\begin{cases} P,\ \vartheta,\ s & \text{(2–field)}, \\ P,\ \vartheta,\ u & \text{(3–field)}, \end{cases} \tag{2.20}$$

thus indicating that the discontinuous waves of the 2–field are vorticity waves (or slip lines, i.e. jumps in the velocity magnitude at the same pressure, entropy and flow direction) and those of the 3–field are entropy waves (i.e. entropy jumps at constant pressure and velocity).

Shock waves are discontinuities in the acoustic wave families (1–field and 4–field) and thanks to the conservation of the tangential velocity (2.18) they can be represented as normal shocks to which a uniform velocity field, parallel to the shock front, is superposed. It is easily checked that if the normal velocity decreases when the shock front is crossed (from the mass and normal momentum relations, the shock is compressive), the shock wave deviates the flow towards the front itself; the opposite occurs if the normal velocity increases (rarefaction shock). This means that $[\vartheta] \gtrless 0$ if $[P] \gtrless 0$ for left-running shock waves (4–field) and $[\vartheta] \lessgtr 0$ if $[P] \gtrless 0$ for right-running shocks (1–field). In addition, from (2.19) with $\rho u_n \neq 0$, it follows the total enthalpy is conserved across the shock. The jump conditions can be combined into the well-known Hugoniot relation

$$[h] - \frac{1}{2}[P](v_- + v_+) = 0, \tag{2.21}$$

where subscripts "$-$" and "$+$" denote the pre-shock and post-shock state, respectively. The Hugoniot relation determines the set (Hugoniot locus) of the thermodynamic states that can be connected by means of a shock wave. In the P–v plane, the Hugoniot locus is commonly referred to as the shock adiabat.

The Rankine-Hugoniot relations must be complemented with suitable admissibility criteria in order to rule out unphysical solutions. The second law of thermodynamics requires that the entropy does not increase across the shock, namely

$$s_+ \geqslant s_-. \tag{2.22}$$

For the shock to be stable against normal perturbations (with respect to its front), the speed ordering relation

$$M_{n+} \leqslant 1 \leqslant M_{n-}, \tag{2.23}$$

where $M_n = u_n/c$ is the normal flow Mach number, must be satisfied (Landau & Lifshitz 1987). Conditions (2.22) and (2.23) have a useful geometrical interpretation in the P–v plane (see Thompson & Lambrakis 1973; Cramer 1989*b*; Kluwick 2001). For an entropy increasing shock, the area between v_- and v_+ under the shock adiabat must be larger than that under the Rayleigh line, the straight line connecting the pre-shock and post-shock states (from equations 2.16-2.17, the slope of the Rayleigh line is $[P]/[v] = -m^2$). The speed ordering relation results in the following condition on the slopes of the shock adiabat and Rayleigh line:

$$\left.\frac{\mathrm{d}P}{\mathrm{d}v}\right|_+ \leqslant \frac{[P]}{[v]} \leqslant \left.\frac{\mathrm{d}P}{\mathrm{d}v}\right|_-, \tag{2.24}$$

where the derivative is taken along the shock adiabat centred on $(P_-,\ v_-)$. A further criterion is that the Rayleigh line must not cut the shock adiabat at interior points; this amounts to require the existence of the one-dimensional thermoviscous profile associated with the normal flow (Cramer 1989*b*). Some consequences of these admissibility criteria are as follows. For convex shock adiabats as in classical gasdynamics, the above requirements are simultaneously satisfied if and only if the shock is pressure-increasing. If the shock adiabat is non-convex, there may appear branches where only rarefaction shocks are admissible (for example, in the region where the shock adiabat is concave) or where one or more of the above conditions fail and therefore no shock wave is admissible.

An additional requirement in multi-dimensional flows is that the shock front is not unstable to transverse perturbations of its front. This condition, introduced by D'yakov (1954) and Erpenbeck (1962), reads

$$-1 \leqslant -\frac{[P]}{[v]}\left(\left.\frac{\mathrm{d}P}{\mathrm{d}v}\right|_+\right)^{-1} \leqslant 1 + 2M_{n+}. \tag{2.25}$$

Assuming $\mathrm{d}P/\mathrm{d}v|_+ < 0$, which is the typical behaviour for most real fluids (Landau & Lifshitz 1987) and it is also observed here throughout, condition (2.25) is satisfied if the speed ordering relation holds. Additional comments concerning the neutral stability to transverse perturbations are provided in the concluding section 7.

2.3. *Composite waves*

Following the loss of genuine nonlinearity due to crossing of the $\Gamma = 0$ locus, in addition to the elementary waves described above, composite waves in which two or more elementary waves propagate as a single entity can possibly occur (Menikoff & Plohr 1989; Kluwick 2001). In order that a composite wave exists, the propagation rays of its elementary waves must be compatible, i.e. they must neither collide nor split. This rules out the case that composite waves be formed by elementary waves of different families. Composite waves can be obtained by stitching together simple waves and shock waves of a given acoustic wave family (of course, two or more adjacent simple waves can be regarded as forming a single simple wave and two or more adjacent discontinuities can be seen as a single discontinuity). In order that a shock wave is adjacent to a simple waves fan, the shock must propagate on the same ray as the edge of the fan, which in turn implies that $M_n = 1$ on the side of the shock wave neighbouring the fan (Cramer *et al.* 1986). By analogy with the nomenclature of one-dimensional unsteady flows, on the side where $M_n = 1$ the shock is said to be sonic. Thus, if $M_{n-} = 1$ the shock is termed pre-sonic and if $M_{n+} = 1$ the shock is post-sonic, while if $M_n = 1$ on both sides, the shock is double-sonic.

If the sonic condition $M_n = 1$ holds on one side of the shock, then relation (2.24) is satisfied with equality on that side, namely the Rayleigh line is tangent to the shock adiabat. At such points on the shock adiabat, the entropy, the mass flux and the slope of the Rayleigh line are all local extrema (see, e.g, Landau & Lifshitz 1987). It can be shown that the thermodynamic state in the sonic side of the sonic shock exhibits $\Gamma < 0$ if the shock is compressive, whereas $\Gamma > 0$ if the shock is rarefactive (Menikoff & Plohr 1989; Kluwick 2001). From the arguments of sections 2.1 and 2.2 on the variation of the flow angle and the pressure across simple waves and shock waves, it is readily obtained that both the flow angle and the pressure are monotonic within a composite wave.

As it is shown below, the topology of Γ in typical BZT fluids imposes a constraint on the maximum number of simple wave fans or shock waves that can possibly appear in a composite wave.

3. Solution of the ramp problem and wave curves

With reference to the ramp problem, we now investigate the wave configurations that can possibly deliver the turning of an upstream supersonic stream in a steady flow. Across entropy and shear waves there is neither mass flux nor deviation of the particle paths (cf. 2.20), therefore the uniform supersonic flow can be turned only across acoustic or shock waves. We immediately note that the presence of both left-running and right-running waves emanating from the ramp corner is not compatible with the boundary conditions imposed by the solid boundary. Thus, if the flow domain is above the solid boundary (e.g., $y > 0$ for the uniform supersonic stream), only a left-running wave can deliver the deflection of the upstream flow and it is at the same time compatible with the condition of flow uniformity at upstream infinity. On the contrary, a right-running wave is required if the the flow domain is below the solid boundary.

Downstream of these wave patterns, a slip line bringing the flow to rest can always be added without changing the overall deflection (several contact waves can be added further downstream). Because we are ultimately interested in describing the structure of the waves that can possibly deliver the turning of the uniform supersonic stream, henceforth we conveniently assume that the angle ϑ_r appearing in (2.6) coincides with the flow deviation across waves of the acoustic fields. That is, the following treatment is valid if one interprets the ramp angle as the turning angle of the uniform supersonic flow (in the absence of downstream contact waves, this is exactly the angle of the solid boundary).

In terms of self-similar wave patterns, the two-dimensional steady supersonic flow involves several analogies with the one-dimensional unsteady case. As is well-known (see, e.g., Godlewski & Raviart 2013), the unsteady one-dimensional Euler equations possess two acoustic characteristic fields corresponding to left-facing and right-facing waves (propagating with speed $u \mp c$, respectively), with a linearly degenerate field corresponding to contact discontinuities (propagating with speed u) in between. In both two-dimensional steady supersonic flows and one-dimensional unsteady flows, the acoustic fields have a similar structure thanks to the following facts. Smooth wave patterns occur, in both cases, in the form of centred fans of acoustic waves. The nonlinearity factor of the acoustic fields, in both cases, are proportional to Γ, which means that the breakdown of simple waves coincides with the condition $\Gamma = 0$ both in two-dimensional steady supersonic flows and in one-dimensional unsteady flows (in turn, this implies that the mechanism of formation of composite waves is the same). Moreover, oblique shocks in two dimensions satisfy the one-dimensional Rankine-Hugoniot relations in the direction normal to the shock front. Thus, steady Prandtl-Meyer fans and oblique shocks are the counterparts of unsteady wave fans and normal shocks, respectively. The correspondence between the elementary wave patterns makes it possible to extend many of the concepts developed for the one-dimensional unsteady case to the steady two-dimensional one. On the other hand, two differences between these frameworks are as follows. In two-dimensional steady flows, self-similar waves can separate hyperbolic and elliptic regions of the flow fields. This change can possibly occur across strong oblique shocks, which drive the Mach number below unity. Secondly, in two-dimensional steady flows, there exists a maximum pressure jump across shock waves, due to the fact that the total enthalpy is constant (cf. 2.13 and 2.19) along streamlines. In contrast, in one-dimensional unsteady flows, any value of the pressure jump can be attained depending on the shock speed.

To formalise the similarity between one-dimensional unsteady flows and two-dimensional steady flows, we introduce here the idea of wave curve for steady two-dimensional flows. In the one-dimensional unsteady flows, the wave curve represents the set of states connected to a given initial state by a self-similar wave of the left-facing or right-facing field (Menikoff & Plohr 1989). In two-dimensional steady flows, the wave curve consists of all the states connected to a given supersonic state by means of a steady self-similar planar wave of the left-running or right-running field. Thus, the wave curve is made of branches corresponding to centred simple waves, shock waves and composite waves. In the context of the supersonic ramp problem, the wave curve computed from the state associated with the uniform supersonic stream embeds all the self-similar waves that can possibly deliver the deflection imposed by the ramp (in the above sense).

Similarly to the one-dimensional case, the construction of wave curves can be simplified by first considering the projection onto the thermodynamic variables; the kinematic quantities are retrieved afterwards. This two-step procedure is the topic of the next sections. Three important observations set the ground for the following treatment:

(i) the projection of a Prandtl-Meyer fan connected to an upstream state A, onto the thermodynamic variables, is a branch of the isentrope passing through the upstream thermodynamic state (cf. the Riemann invariants 2.13). Given, e.g., the downstream pressure P_{B}, all the thermodynamic quantities downstream of the fan are readily determined. The kinematic quantities (e.g. u_{B} and ϑ_{B}) are computed by imposing the conservation of the total enthalpy h^t and of the Riemann invariant $\theta \mp \nu$ of opposite sign;

(ii) shock waves connected to state A project, in the thermodynamic plane, onto a branch of the Hugoniot locus passing through the upstream thermodynamic state (cf. equation 2.21). Given, e.g., the downstream pressure, the downstream density is computed from (2.21) and, from those, each downstream thermodynamic quantity and the mass flux $m = (-[P]/[v])^{1/2}$. The shock angle β_s and flow deflection angle ϑ_{B} (with respect to the upstream flow direction) are computed from $m = \rho_{\mathrm{A}} u_{\mathrm{A}} \sin\beta_s$ and $\rho_{\mathrm{A}} \tan\beta_s = \rho_{\mathrm{B}} \tan(\beta_s - \vartheta_{\mathrm{B}})$, respectively.

(iii) Prandtl-Meyer fans cannot be continued at states of linear degeneracy $\Gamma = 0$, because there the characteristic lines fold. If a further pressure variation is imposed, this is accomplished by means of a composite wave in which the fan terminates in a pre-sonic oblique shock (Menikoff & Plohr 1989). The shock-wave branch of the wave curve cannot be continued at entropy extrema, whereby the Rayleigh line is tangent to the shock adiabat, because a further variation in the post-shock pressure would lead to violation of the speed ordering relation (2.23). The wave curve beyond an entropy extremum in the Hugoniot locus is continued as a composite shock/fan wave. By collecting the states downstream of the composite wave, a composite locus is obtained (see also Kluwick 2001).

4. Wave curves in the thermodynamic plane

Let us consider the structure of the wave curve projection onto the thermodynamic variables, say the P–v plane. Remarks (i) and (ii) in the previous section imply that for a given upstream state, the projected wave curve is a subset of the one-dimensional unsteady counterpart. The kinematic state of the upstream flow, through the value of the total enthalpy which remains constant throughout the flow field and limits the maximum pressure jump across oblique shocks, determines endpoints of the wave curve. This suggests that one can use the well-established results for the one-dimensional unsteady case (replacing, of course, unsteady wave fans with Prandtl-Meyer waves and unsteady normal shocks with steady oblique shocks) to determine the underlying structure of the wave curve in the thermodynamic plane, namely the extended (i.e. drawn up to vacuum and infinite pressure) wave curves. The upstream kinematic is then taken into account (in the following section) to determine endpoints of the waves curves.

In order to illustrate the different types of wave curves in a typical BZT fluid, the polytropic van der Waals model (namely with constant isochoric specific heat) of a molecularly complex fluid is considered. Several previous studies have proved the soundness of the adoption of this simple model for qualitative analysis, owing to the fact that the negative-Γ region is well captured (Thompson & Lambrakis 1973; Kluwick 2001; Guardone *et al.* 2004; Guardone & Argrow 2005). The fluid selected for this purpose is siloxane MDM (octamethyltrisiloxane, $C_8H_{24}0_2Si_3$) with $c_v/R = 57.69$, where c_v is the isochoric heat capacity and R is the gas constant.

Five thermodynamic states are chosen along the same isentrope s_{A} crossing the negative-Γ region while remaining in the single-phase, as shown in figure 1a. The corresponding extended wave curves in the P–v plane are shown in figure 1b-f. These are now detailed.

Case 1 – figure 1b. Thermodynamic state A_1 is located on the right-hand side of the negative-Γ region. Thus, the rarefaction branch of the extended wave curve through A_1 is the isentrope containing A_1, associated with elementary Prandtl-Meyer waves connected to A_1. On the other hand, the compressive branch of the wave curve coincides with the shock adiabat centred on A_1, associated with oblique shock waves. Note that, despite the shock adiabat crosses the negative-Γ region and it is non-convex, no entropy extrema occur. Graphically, this means the Rayleigh line (straight line connecting the pre-shock and post-shock states) is never tangent to the shock adiabat at the post-shock state. The same wave curve configuration (compression shock and rarefaction fan branches) is observed whenever the isentrope passing through the upstream state is convex (see, e.g., Kluwick 2001).

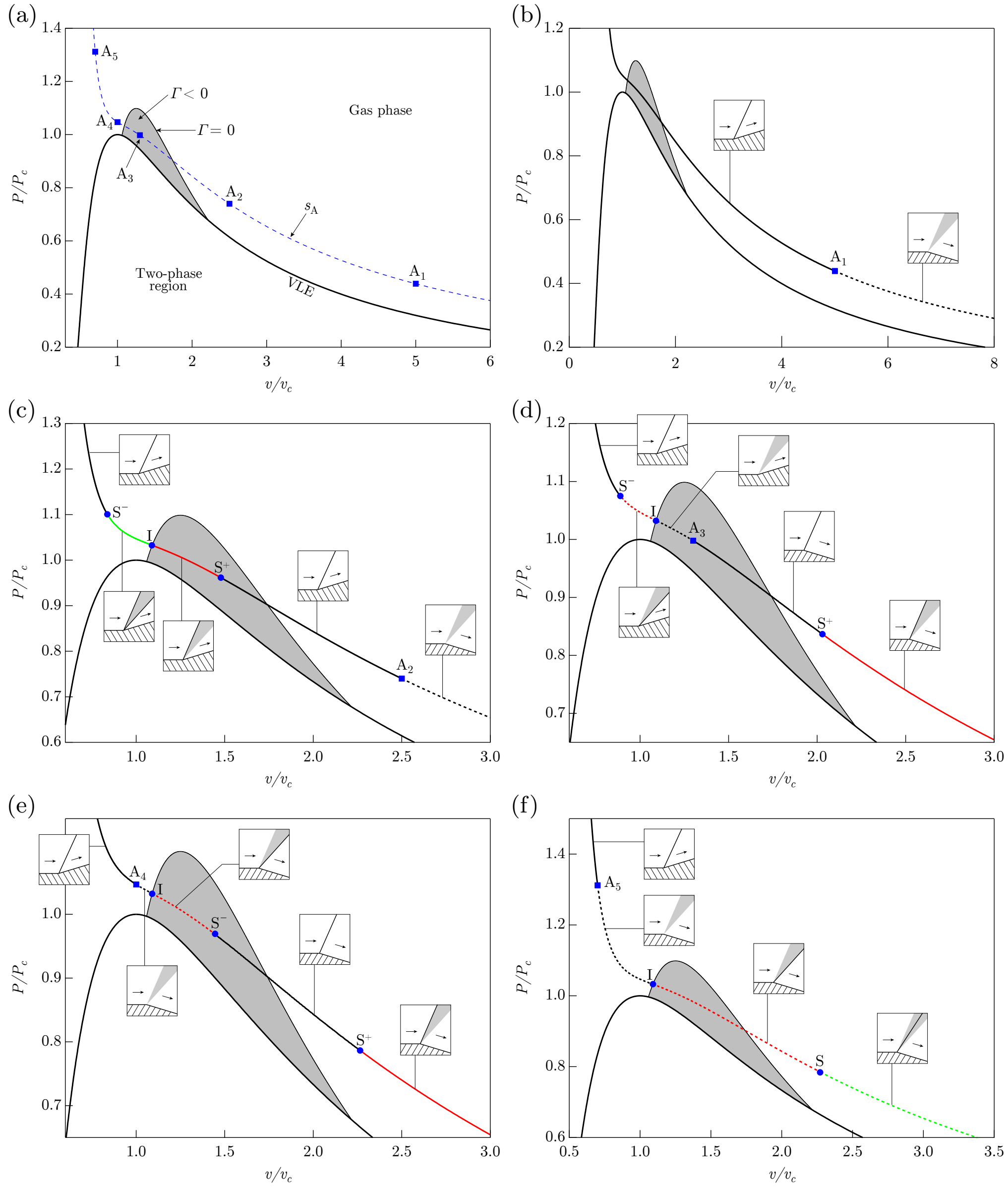

FIGURE 1. Extended wave curves in the pressure–specific volume diagram (subscript c indicates critical-point quantities) computed from the polytropic van der Waals model of fluid MDM. (a) The selected upstream states, chosen along an isentrope crossing the negative-Γ region (shaded area). (b)-(f) Extended wave curve for each upstream state. Wave configurations: —— shock, —— shock/fan, —— shock/fan/shock, - - - fan, - - - fan/shock, - - - fan/shock/fan. Point S^+: downstream state of post-sonic oblique shock; point S^-: downstream state of pre-sonic oblique shock; point S: downstream state of double-sonic oblique shock; point I: intersection between the local isentrope and $\Gamma = 0$ locus. Attached to each branch is a qualitative sketch of the (left-running) wave configuration in the physical plane, where thick lines denote oblique shocks and shaded areas denote wave fans.

Case 2 – figure 1c. Similarly to case 1, thermodynamic state A_2 is on the right-hand side of the negative-Γ region. The rarefaction branch of the wave curve, therefore, is as in the previous case. On the contrary, the compression branch is significantly different. The wave curve is still, for moderate pressure rises, the locus of the oblique shocks connected to A_2. In contrast to case 1, however, there there exist a downstream pressure (point S^+) for which the entropy along the shock adiabat reaches a local maximum (i.e. the Rayleigh line is tangent to the shock adiabat at S^+); shock A_2-S^+ is indeed a post-sonic compression shock. As mentioned in §3, the wave curve is continued along the isentrope passing through S^+, for a composite oblique shock/Prandtl-Meyer fan combination. The fan in the composite wave cannot be continued beyond point I, where the isentrope through S^+ intersect the $\Gamma = 0$ locus, for the characteristic lines would fold. Beyond point S^+, the wave curve is continued by inserting a pre-sonic oblique shock adjacent to the fan. Thus, the corresponding wave configuration is a composite of the type oblique shock/Prandtl-Meyer fan/oblique shock. With increasing downstream pressure, the terminating shock becomes stronger and the wave fan weaker. Ultimately, at point S^- the fan disappears; shock A_2-S^- can be seen as the composition of the post-sonic shock A_2-S^+ and the pre-sonic shock S^+-S^-. For downstream pressures larger than the value at point S^-, a single oblique shock configuration is recovered.

Case 3 – figure 1d. If the upstream thermodynamic state is selected in the negative-Γ region, such as point A_3, the rarefaction branch of the wave curve is the shock adiabat centred on the initial state (rarefaction oblique shock waves), up to the point S^+ where a post-sonic rarefaction shock occurs. Beyond this point, the wave curve is continued along the isentrope through S^+, for a composite oblique shock/Prandtl-Meyer fan combination. On the other hand, the compression branch of the wave curve is initially the isentrope through A_3 (compression Prandtl-Meyer waves), up to the point I where this isentrope intersects the $\Gamma = 0$ locus. The wave curve is continued by inserting a pre-sonic shock adjacent to the fan, for a Prandt-Meyer fan/oblique shock composite configuration in the physical plane. With increasing downstream pressure, the terminating oblique shock becomes stronger and the wave fan weaker; downstream pressures beyond point S^-, at which a pre-sonic compression shock occurs, are accomplished by a single oblique shock configuration.

Case 4 – figure 1e. State A_4 lies on the left-hand side of the negative-Γ region. Therefore, the compression branch of the wave curve through state A_4 is the shock adiabat centred on A_4. The rarefaction branch is initially the isentrope through state P_4, up to the point where the $\Gamma = 0$ locus is encountered. The wave curve is continued by inserting a pre-sonic shock adjacent to the fan. For the downstream pressure corresponding to point S^- (pre-sonic rarefaction shock A_4-S^-), the Prandtl-Meyer fan disappears and a single oblique shock occurs. By decreasing the downstream pressure, the post-shock normal Mach number decreases and at point S^+ it is equal to unity (post-sonic oblique shock A_4-S^+). Smaller downstream pressures are achieved by means of a composite oblique shock/Prandtl-Meyer fan combination, for the wave curve beyond point S^+ is indeed the isentrope through S^+.

Case 5 – figure 1f. The wave curve configuration is the same as in case 4, except that for the downstream pressure corresponding to point S, a composite fan/double-sonic shock configuration is observed (see also Zamfirescu *et al.* 2008). The wave curve of point A_5 is continued, beyond point S, along the isentrope through S. The associated wave in the physical plane is the composite fan/shock/fan configuration.

5. Polar representation of the wave curves

Moving from the identification of the different types of extended wave curves in the space of thermodynamic variables, in this section we describe the wave curves in the common pressure–deflection diagram, where the downstream pressure P_{B} is plotted against the downstream deflection angle ϑ_{B} that the wave generates. The representation of the wave curve in these variables is necessary connected with the kinematic quantities along the wave curves. Here it is possible to evaluate the effect of the kinematic state of the upstream flow, in particular how this determines the endpoints of the wave curve (which are associated with the maximum pressure jump across oblique shocks). The upstream kinematic state is accounted for in terms of upstream Mach number M_{A}. In order to analyse the possible configurations of the wave curves along with the influence of M_{A}, we select the same upstream thermodynamic states considered in the previous section and we draw the wave curve projection in the P_{B}–ϑ_{B} diagram for different values of M_{A}, as shown in figure 2. Without loss of generality, only left-running wave curves are considered, as the right-running wave is just the reflection, through the $\vartheta_{\mathrm{B}} = 0$ axis, of the left-running counterpart.

Case 1 – figure 2b. On a qualitative basis, this is the classical case. The rarefaction branch (Prandtl-Meyer waves) extends to vacuum conditions (eventually the saturated phase boundary is crossed), where the deflection angle attains a finite limit value. The pressure rise along the compression branch is limited by the normal shock wave ($\beta_s = 90°, \vartheta_{\mathrm{B}} = 0$) from the upstream state. By increasing the upstream Mach number, and therefore the total enthalpy of the stream, the maximum pressure jump increases. As is well-known (Thompson 1988, see, e.g.,), for a given $\vartheta_{\mathrm{B}} > 0$ two oblique shocks can possibly occur, which are named the weak and the strong (based on the pressure jump) solutions.

Case 2 – figure 2c. While the rarefaction branch is qualitatively similar to case 1, there exists a limit value of the upstream Mach number, $M_{\mathrm{A}}^{\mathrm{tr}}$, marking the transition between two qualitatively different compression-branch configurations. If $1 < M_{\mathrm{A}} < M_{\mathrm{A}}^{\mathrm{tr}}$, the ordinary shock polar, similar to case 1, occurs. For $M_{\mathrm{A}} > M_{\mathrm{A}}^{\mathrm{tr}}$, along the compressive branch of the wave curve the following sequence is encountered, in the direction of increasing downstream pressure: oblique shock, oblique shock/Prandtl-Meyer fan, oblique shock/Prandtl-Meyer fan/oblique shock, oblique shock. The transitional wave curve is distinguished because the normal shock delimiting the first shock branch exhibits the sonic downstream state $M_{n\mathrm{B}} = M_{\mathrm{B}} = 1$, namely the post-shock thermodynamic state coincides with point S^+ in figure 1c. By enforcing the Rankine-Hugoniot relations for a normal shock wave, the transitional Mach number is therefore computed as

$$M_{\mathrm{A}}^{\mathrm{tr}} = \frac{1}{\rho_{\mathrm{A}} c_{\mathrm{A}}} \sqrt{\frac{P_{\mathrm{S}^+} - P_{\mathrm{A}}}{v_{\mathrm{A}} - v_{\mathrm{S}^+}}}, \tag{5.1}$$

where P_{S^+} and v_{S^+} are the pressure and specific volume, respectively, at point S^+. For upstream Mach numbers slightly larger than the transitional value, ϑ_{B} exhibits three stationary points along the wave curve (two local maxima with a minimum in between). Thus, up to four different wave configurations can provide the same flow deflection.

Case 3 – figure 2d. A single qualitative configuration is observed for the compression side of the wave curve, which is composed by three branches: Prandtl-Meyer fan, Prandtl-Meyer fan/oblique shock, oblique shock (increasing downstream pressure). Two qualitatively different configurations are possible for the rarefaction branch, based on the value of the upstream Mach number. As in the previous case, a threshold Mach number $M_{\mathrm{A}}^{\mathrm{tr}}$ exists, such that the ordinary shock polar (though for rarefaction shocks) occurs

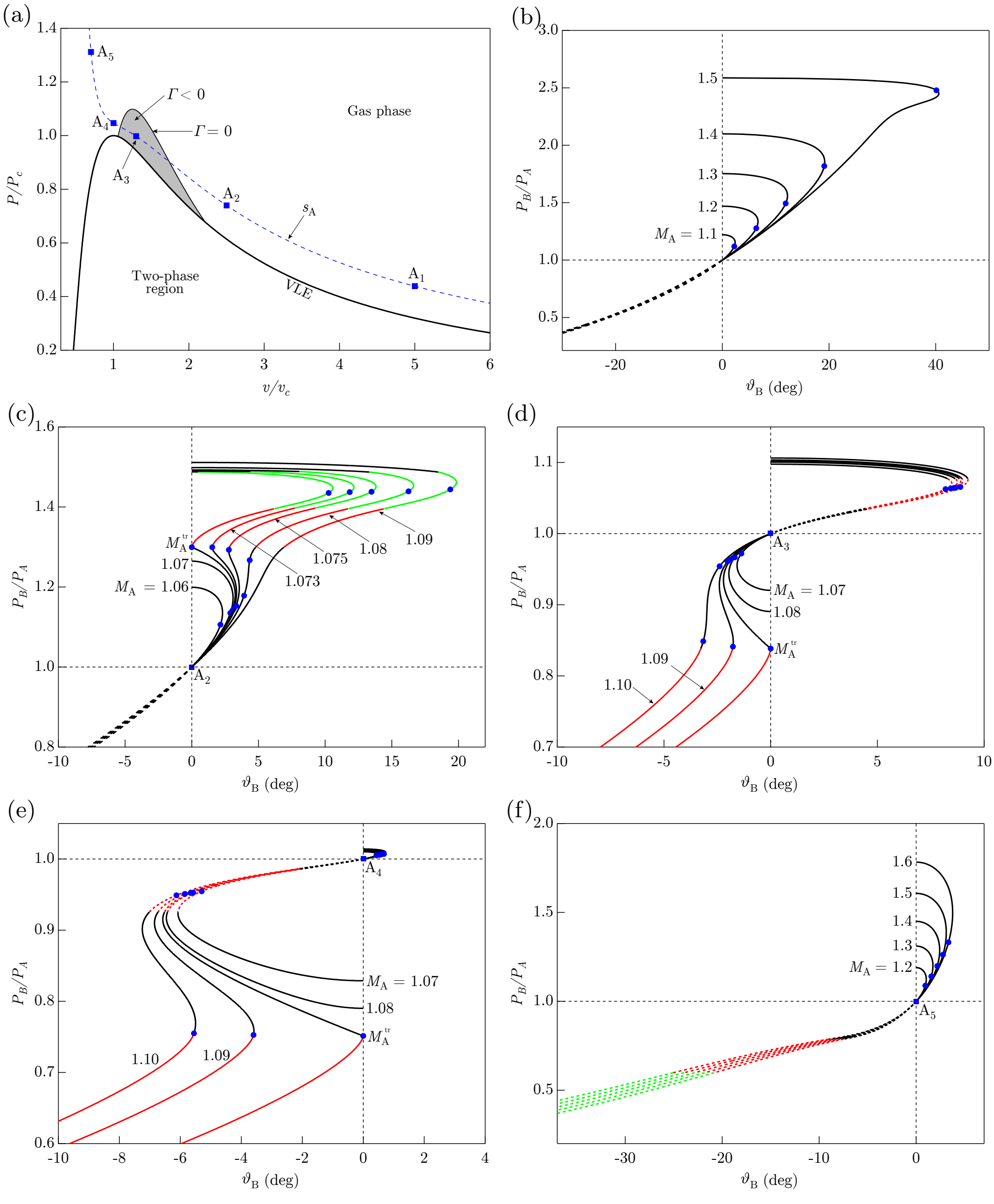

FIGURE 2. Left-running wave curves in the pressure–deflection diagram computed from the polytropic van der Waals model of fluid MDM. (a) The selected thermodynamic upstream states, chosen along an isentrope crossing the negative-Γ region (shaded area). (b)-(f) Wave curve for each upstream thermodynamic state and different upstream Mach numbers. For each case, the downstream pressure P_B is scaled using the corresponding upstream pressure P_A. Wave configurations: —— shock, —— shock/fan, —— shock/fan/shock, - - - fan, - - - fan/shock, - - - fan/shock/fan. Symbol • denotes downstream sonic points ($M_B = 1$).

if $M_A < M_A^{tr}$. Note that, for $M_A < M_A^{tr}$, the largest pressure drop is attained across the normal rarefaction shock from the upstream state, i.e. the rarefaction branch does not extend to vacuum. The transitional curve is again determined by the occurrence of a post-sonic normal shock wave (downstream thermodynamic state S^+ in figure 1d). Therefore, formula (5.1) applies for the computation of $M_{\mathrm{A}}^{\mathrm{tr}}$.

Case 4 – figure 2e. The compression branch is the classical polar of oblique shocks. Two qualitatively different configurations of the rarefaction branch can possibly occur, again depending on M_{A}. If $M_{\mathrm{A}} < M_{\mathrm{A}}^{\mathrm{tr}}$, the configurations are, in the direction of decreasing downstream pressure: Prandtl-Meyer fan, Prandtl-Meyer fan/oblique shock, oblique shock. If $M_{\mathrm{A}} > M_{\mathrm{A}}^{\mathrm{tr}}$, the wave curve extends to vacuum via an additional oblique shock/Prandtl-Meyer fan configuration. Similarly to cases 2 and 3, the transitional wave curve is distinguished by the occurrence of a post-sonic normal shock wave (downstream thermodynamic state S^+ in figure 1e), so that $M_{\mathrm{A}}^{\mathrm{tr}}$ is again computed from relation (5.1).

Case 5 – figure 2f. For case 5 a single wave curve configuration is possible. The compression branch comprises the ordinary shock polar. For decreasing downstream pressures, the rarefaction branch consists of: Prandtl-Meyer fan, Prandtl-Meyer fan/oblique shock, Prandtl-Meyer fan/oblique shock/Prandtl-Meyer fan.

All the above shock solutions satisfy the stability conditions specified in §2.2. However, it was shown by Kontorovich (1958) that in the range

$$\frac{1 - M_{n+}^2 - (v_-/v_+)M_{n+}^2}{1 - ([v]/v_+)M_{n+}^2} < -\frac{[P]}{[v]}\left(\left.\frac{\mathrm{d}P}{\mathrm{d}v}\right|_+\right)^{-1} \leqslant 1 + 2M_{n+} \tag{5.2}$$

the shock front is only neutrally stable against transverse perturbations and can spontaneously emit acoustic waves (see also Fowles 1981). Acoustic emission is predicted to occur in molecularly complex fluids, for shock waves originating in the thermodynamic region close to the saturation curve and critical point (Alferez & Touber 2017). We note that inequalities (5.2) are satisfied if the sonic point in the pressure–deflection polar is at larger pressures than the maximum turning angle (Menikoff & Plohr 1989). One such case is the oblique shock polar marked by $M_{\mathrm{A}} = 1.5$ in figure 2b.

6. Upstream-state map of the wave-curve types

Having described the different configurations for the compression and rarefaction branches of the waves curves for steady, two-dimensional and supersonic (possibly mixed supersonic/subsonic across strong oblique shocks) flows, we can now investigate the necessary conditions that the upstream state must satisfy in order to produce a specific wave-curve configuration. Ultimately, the purpose of this section is to determine a map of the upstream states leading to the different types of wave curve identified in the previous section.

For future convenience, the wave curve types are classified according to their qualitative structure, as shown in table 1. Seven different wave-curve configurations are singled out, which include the classical configuration $\mathcal{C}$ and six different non-classical configurations $\mathcal{N}_i$, $i = 1, \ldots, 6$. The classical wave curve $\mathcal{C}$ is the one depicted in figure 2b and in figure 2c for $M_{\mathrm{A}} < M_{\mathrm{A}}^{\mathrm{tr}}$; $\mathcal{N}_1$ is found in 2c if $M_{\mathrm{A}} > M_{\mathrm{A}}^{\mathrm{tr}}$; $\mathcal{N}_2$ and $\mathcal{N}_3$ occur in figure 2d for $M_{\mathrm{A}} < M_{\mathrm{A}}^{\mathrm{tr}}$ and $M_{\mathrm{A}} > M_{\mathrm{A}}^{\mathrm{tr}}$, respectively; $\mathcal{N}_4$ and $\mathcal{N}_5$ in figure 2e for $M_{\mathrm{A}} < M_{\mathrm{A}}^{\mathrm{tr}}$ and $M_{\mathrm{A}} > M_{\mathrm{A}}^{\mathrm{tr}}$, respectively; finally $\mathcal{N}_6$ is the configuration shown in figure 2f.

In order to reduce the complexity associated with the dependence of the wave curves on three upstream quantities (two thermodynamic quantities, e.g. P_{A}, v_{A} and a kinematic or mixed one, e.g. M_{A}), we first consider upstream thermodynamic states along exemplary isentropes, as shown in figure 3, and we analyse the conditions that determine the transition between different wave curve configurations.

Isentrope a in figure 3 is representative of the scenario observed for convex isentropes.

Wave-curve type	Compression branch	Rarefaction branch
$\mathcal{C}$	S	F
$\mathcal{N}_1$	S–SF–SFS–S	F
$\mathcal{N}_2$	F–FS–S	S
$\mathcal{N}_3$	F–FS–S	S–SF
$\mathcal{N}_4$	S	F–FS–S
$\mathcal{N}_5$	S	F–FS–S–SF
$\mathcal{N}_6$	S	F–FS–FSF

Table 1. Classification of the wave curves. S: oblique shock; F: Prandtl-Meyer fan; SF: composite oblique shock/Prandtl-Meyer fan; SFS: composite oblique shock/Prandtl-Meyer fan/oblique shock; FS: composite Prandtl-Meyer fan/oblique shock; FSF: composite Prandtl-Meyer fan/oblique shock/Prandtl-Meyer fan. In the compression branch, the configurations encountered are listed in the order of increasing downstream pressure, while in the rarefaction branch they are in the order of decreasing downstream pressure.

As such, only classical wave curves can originate from upstream thermodynamic states along these curves and any given upstream Mach number $M_{\mathrm{A}} > 1$.

Isentrope b is the same used for the parametric studies of the previous sections. It is representative of the scenario arising from isentropes that cross the negative-Γ region while remaining in the single-phase. At sufficiently low upstream pressure, only the classical configuration shown in figure 1b and 2b can occur. By increasing the pressure along the selected isentrope, point $\mathrm{PS}_{\mathrm{max}}$ is encountered at which the wave curve first includes a post-sonic compression shock. It can be shown (Menikoff & Plohr 1989) that the post-sonic compression shock arising from $\mathrm{PS}_{\mathrm{max}}$ exhibits $\Gamma_{\mathrm{B}} = 0$. Also, it is the post-sonic compression shock of largest intensity (e.g., pressure or entropy jump) among those originating from the selected isentrope. For pressures included between $\mathrm{PS}_{\mathrm{max}}$ and I'_b (low-density intersection with the $\Gamma = 0$ locus), the extended wave curve in the thermodynamic plane is qualitatively similar to that of figure 1c. As shown in §5, two different types of wave curve ($\mathcal{C}$ and $\mathcal{N}_1$) can occur based on the value of the upstream Mach number. The threshold Mach number between these two configurations, as computed from relation (5.1), is graphically highlighted in figure 3 using the colormap. For upstream states exhibiting $\Gamma_{\mathrm{A}} < 0$, wave curves of type $\mathcal{N}_2$ or $\mathcal{N}_3$ can be observed. The same transitional criterion based on M_{A} applies and is again represented on the isentrope itself in figure 3. The branch of isentrope b on the left-hand side of point I''_b (high-density intersection with the $\Gamma = 0$ locus), is two sections by point DS, which denotes the occurrence of a double-sonic shock (Zamfirescu *et al.* 2008). Between I''_b and DS, double-sonic shocks from upstream states along the chosen isentrope are not possible. Therefore, configurations $\mathcal{N}_2$ or $\mathcal{N}_3$ can occur based on M_{A}. Beyond point DS, the wave curve is of type $\mathcal{N}_6$ only.

In the present discussion, we also consider the single-phase portions of isentropes crossing the saturation curve. The case of isentropes crossing both the negative-Γ region and the saturation curve is the one labelled c in figure 3. Non-classical configurations can possibly exist only in the neighbourhood of point I'_c. The branch $\mathcal{C}/\mathcal{N}_1$, in this case, is bounded below by point $\mathrm{PS}_{\mathrm{sat}}$, where the post-sonic shock required for the existence of $\mathcal{N}_1$ configurations features post-shock saturated conditions (namely, the post-shock thermodynamic state lies on the vapour-liquid equilibrium curve). Finally, for isentropes such as case d in figure 3, which cross the phase boundary but do not cross the negative-Γ region, only the classical wave curve configuration is predicted to occur.

By applying the above procedure to each possible isentrope, a map, in terms of

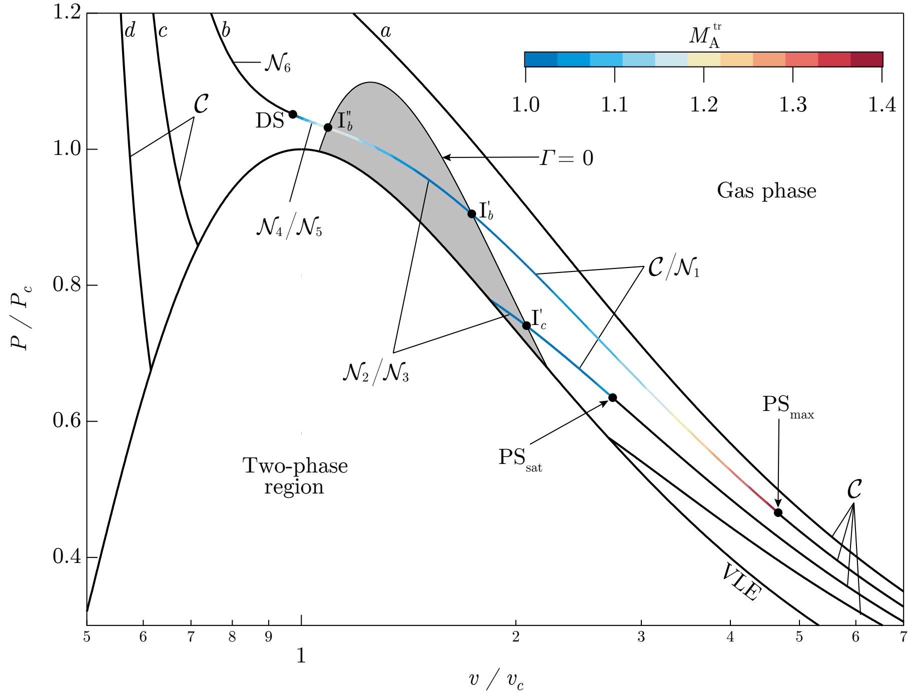

FIGURE 3. Wave curve configurations for upstream thermodynamic states along selected isentropes, as computed from the polytropic van der Waals model of fluid MDM. The colormap indicates the transitional upstream Mach number (cf. relation 5.1) for the branches where two different configurations are possible.

thermodynamic quantities and Mach number, of the upstream states leading to each wave curve configuration is obtained, see figure 4. In the P–v plane, the thermodynamic region associated with non-classical wave curves is bounded above by the isentrope s_τ tangent to the $\Gamma = 0$ locus and by the curve $\mathrm{PSL_{max}}$. The latter is obtained by collecting all the upstream states $\mathrm{PS_{max}}$ leading to post-sonic shocks of maximal intensity along a given pre-shock isentrope (as defined above). In a similar fashion, the curve $\mathrm{PSL_{sat}}$ is computed as the locus of thermodynamic states $\mathrm{PS_{sat}}$, for each isentrope crossing both the negative-Γ region and the saturation curve. The $\mathrm{PSL_{sat}}$ bounds from below the region for non-classical wave curves, along with the saturation curve itself and the isentrope s_{vle} tangent to the latter. The locus $\Gamma = 0$ marks the transition between the regions $\mathcal{C}/\mathcal{N}_1$ and $\mathcal{N}_2/\mathcal{N}_3$ and between the regions $\mathcal{N}_2/\mathcal{N}_3$ and $\mathcal{N}_4/\mathcal{N}_5$. The DSL, which separates the regions $\mathcal{N}_4/\mathcal{N}_5$ and $\mathcal{N}_6$, is obtained by collecting the pre-shock states of double sonic shocks (DS). The DSL shown in figure figure 4 is indeed a portion of the Double-Sonic Locus defined by Zamfirescu *et al.* (2008). Outside the above-described bounds, only classical wave curves can take place.

We assert that the present findings do not depend on the specific choice of the thermodynamic model, insofar as they result from the existence of a finite negative-Γ region in the vapour phase. To support this claim, the upstream-state map of the wave curves for fluid MD_4M (tetradecamethylhexasiloxane, $C_{14}H_{42}0_5Si_6$), as computed from the state-of-the-art multi-parameter equation of state of (König & Thol 2018) available via the REFPROP library (Lemmon *et al.* 2013), is reported in figure 5 and shows excellent qualitative agreement with the picture given by the simple van der Waals model.

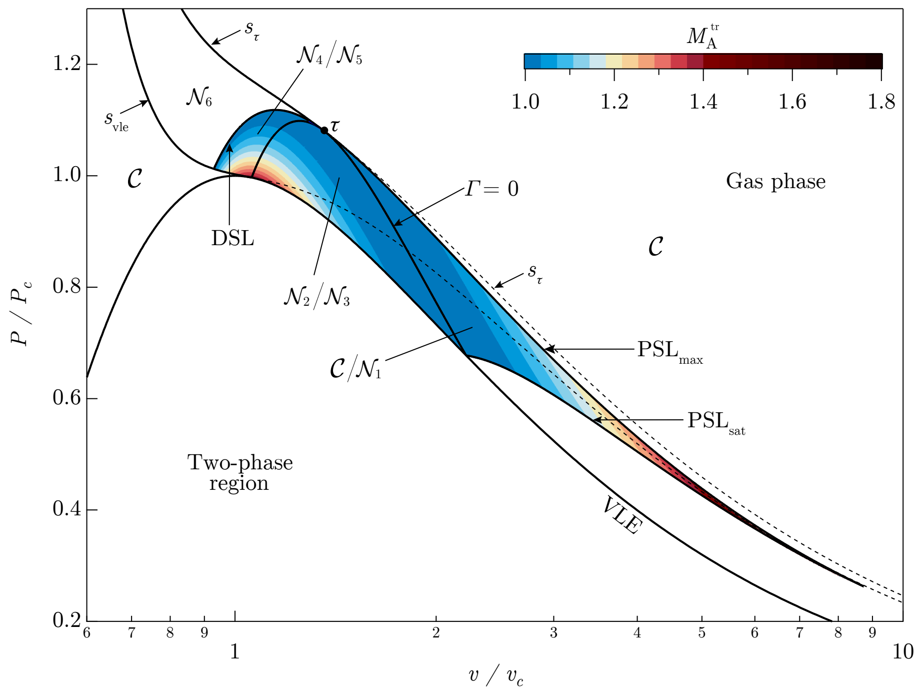

FIGURE 4. Upstream-state map of the wave curves in the P–v plane, as computed from the polytropic van der Waals model of fluid MDM. Superposed is the value of transitional upstream Mach number (cf. relation 5.1) for the regions where two different configurations are possible.

7. Concluding remarks

The general properties of self-similar oblique waves (left-running or right-running with respect to the fluid particle velocity) in steady, inviscid, single-phase Bethe-Zel'dovich-Thompson vapours were studied. The developed theoretical framework concentrates on compressive and rarefactive ramps/wedges in both the classical and non-classical gasdynamic context, which are the building blocks of steady planar supersonic flows. Due to the possibly non-convex character of isentropes and shock adiabats in the pressure–specific volume diagram, several oblique-wave patterns are identified which are not admissible in the classical theory of gasdynamics: the composite shock/fan, fan/shock, shock/fan/shock and fan/shock/fan combinations. Moreover, the elementary oblique waves originating from thermodynamic states in the negative-Γ exhibit inverse gasdynamic behaviour, namely oblique shocks carry an expansion while Prandtl-Meyer fans are compressive.

The two-dimensional ramp problem was described moving from the one-dimensional Riemann problem, thus allowing us to exploit most of the techniques developed for self-similar flow in one dimension. Accordingly, the concept of wave curve for steady two-dimensional flow, which is the counterpart the wave curve in the one-dimensional Riemann problem, was introduced. Within the present context, the wave curve consists of all the states (in terms of thermodynamic and kinematic quantities) that can possibly be connected to a given supersonic state by means of a steady, two-dimensional and self-similar wave. A two-step procedure was adopted to compute the wave curve: the projection onto the thermodynamic variables was first considered, since it represents a

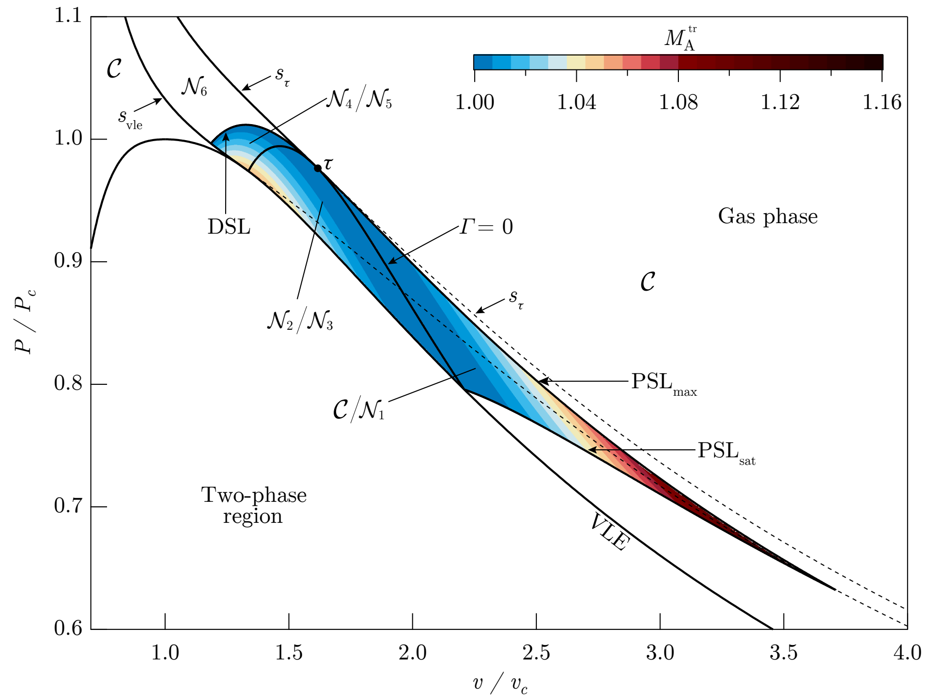

FIGURE 5. Upstream-state map of the wave curves in the P–v plane, as computed from the reference thermodynamic model of fluid $\mathrm{MD_4M}$ (König & Thol 2018), available via the REFPROP library (Lemmon *et al.* 2013). Superposed is the value of transitional upstream Mach number (cf. relation 5.1) for the regions where two different configurations are possible.

subset of the unsteady one-dimensional counterpart, and afterwards all the kinematic quantities were retrieved.

The different types of wave curves were illustrated my means of a parametric study in the space of the upstream thermodynamic quantities (e.g., pressure and specific volume) and Mach number, using the van der Waals gas model (with constant isochoric specific heat) of a molecularly complex fluid. Seven different wave curve configurations were singled out, which include the classical case ($\mathcal{C}$) and six non-classical cases ($\mathcal{N}_1$, $\mathcal{N}_2$, $\mathcal{N}_3$, $\mathcal{N}_4$, $\mathcal{N}_5$, $\mathcal{N}_6$). The conditions leading to the transition between the different types of wave curve were analysed. This led to the definition of a map, in the parameter space of the thermodynamic quantities and Mach number, of the upstream states leading to each type of wave curve. Most important, it was shown that the domain of the thermodynamic states leading to wave curves of non-classical type is significantly larger than the negative-Γ region in which inverse gasdynamic behaviour is expected to occur. As the peculiar oblique-wave properties stem from the occurrence of a negative-Γ region in the vapour phase, we expect that the results obtained from the simple van der Waals model apply to diverse thermodynamic models of BZT fluids. The computation of the upstream-state map of the wave curves using the state-of-the-art thermodynamic model of fluid $\mathrm{MD_4M}$ corroborates this statement.

In contrast with the classical case, if the non-classical configuration $\mathcal{N}_1$ is generated, up to four different wave patterns corresponding to the same ramp angle can possibly occur. Moreover, for the non-classical configurations $\mathcal{N}_2$, $\mathcal{N}_3$, $\mathcal{N}_4$ and $\mathcal{N}_5$, the deviation angle does not vary monotonically with the downstream pressure along the expansion branch, where up to three different wave patterns can possibly occurs which correspond to the same ramp angle. The question arises whether the solutions other than the strong shock are admissible. An important problem for further study is therefore the stability of composite waves.

In closing, we note that the current theoretical framework can be conveniently applied to the study of shock reflections and shock interactions, which will be the topic of future studies.

Acknowledgements

This research is supported by ERC Consolidator Grant N. 617603, Project NSHOCK, funded under the FP7-IDEAS-ERC scheme.

Appendix A. Eigenvalue problem for the steady 2D Euler equations

The steady two-dimensional Euler equations (2.1) can be written in quasi-linear form as

$$A_x(q)\partial_x q + A_y(q)\partial_y q = 0, \tag{A 1}$$

in which $A_x(q) = D_q F_x(q)$ and $A_y(q) = D_q F_y(q)$ are the Jacobians of the fluxes, namely

$$A_x(q) = \left(\frac{\partial F_{xi}}{\partial q_j}(q)\right)_{1\leqslant i,j\leqslant 4}, \tag{A 2}$$

$$A_y(q) = \left(\frac{\partial F_{yi}}{\partial q_j}(q)\right)_{1\leqslant i,j\leqslant 4}, \tag{A 3}$$

where F_{xi} and F_{yi} denote the i-th element of F_x and F_y, respectively, and q_j is the j-th element of q.

The generalized eigenvalue problem

$$\Big(A_y(q) - \lambda_k(q)A_x(q)\Big)r_k(q) = 0, \tag{A 4}$$

where λ_k and r_k indicate the k-th eigenvalue and right eigenvector, respectively, is associated with the hyperbolicity of (2.1) and with the notions of genuinely nonlinear or linearly degenerate characteristic fields through the derived quantity $\alpha_k(q) = D_q\lambda_k(q)\cdot r_k(q)$, known as the nonlinearity factor of the k-th field. Because the properties of the characteristic fields do not depend on the chosen conservative or nonconservative form of the nonlinear hyperbolic system, a suitable change of variables may be advantageous (Godlewski & Raviart 2013). Using the map

$$(\rho, \rho u_x, \rho u_y, \rho e + \rho u^2/2) \mapsto (P, u, \vartheta, s), \tag{A 5}$$

where $\vartheta = \tan^{-1}(u_y/u_x)$ is the angle formed by the particle path with the x-axis, the Jacobians in the mapped variables can be written as (the same notation is maintained for simplicity)

$$A_x(q) = \begin{bmatrix} u\cos\vartheta/c^2 & \rho\cos\vartheta & -\rho u\sin\vartheta & u\cos\vartheta\left(\frac{\partial\rho}{\partial s}\right)_P \\ 1/\rho & u\cos^2\vartheta & -u^2\cos\vartheta\sin\vartheta & 0 \\ 0 & u\cos\vartheta\sin\vartheta & u^2\cos^2\vartheta & 0 \\ 0 & 0 & 0 & u\cos\vartheta \end{bmatrix}, \tag{A 6}$$

$$A_y(q) = \begin{bmatrix} u\sin\vartheta/c^2 & \rho\sin\vartheta & \rho u\cos\vartheta & u\sin\vartheta\left(\frac{\partial\rho}{\partial s}\right)_P \\ 0 & u\cos\vartheta\sin\vartheta & -u^2\sin^2\vartheta & 0 \\ 1/\rho & u\sin^2\vartheta & u^2\cos\vartheta\sin\vartheta & 0 \\ 0 & 0 & 0 & u\sin\vartheta \end{bmatrix}. \tag{A 7}$$

For supersonic flows, namely if $M > 1$, the eigenvalue problem (A 4) gives the well-known eigenvalues

$$\lambda_1(q) = \tan(\vartheta - \mu), \quad \lambda_{2,3}(q) = \tan\vartheta, \quad \lambda_4(q) = \tan(\vartheta + \mu), \tag{A 8}$$

and eigenvectors

$$r_1(q) = \begin{pmatrix} -\rho u^2 \\ \dfrac{u}{\sqrt{M^2-1}} \\ 0 \end{pmatrix}, \quad r_2(q) = \begin{pmatrix} 0 \\ 1 \\ 0 \\ 0 \end{pmatrix}, \quad r_3(q) = \begin{pmatrix} 0 \\ 0 \\ 0 \\ 1 \end{pmatrix}, \quad r_4(q) = \begin{pmatrix} \rho u^2 \\ \dfrac{-u}{\sqrt{M^2-1}} \\ 0 \end{pmatrix}, \tag{A 9}$$

in which the angle $\mu = \sin^{-1}(1/M)$, is the Mach angle. In the mapped variables, the partial derivatives of the eigenvalues read

$$D_q\lambda_1(q) = \frac{1+\tan^2(\vartheta-\mu)}{\sqrt{M^2-1}}\left(-\frac{\Gamma-1}{\rho c^2}, \frac{1}{u}, \sqrt{M^2-1}, -\frac{1}{c}\left(\frac{\partial c}{\partial s}\right)_P\right), \tag{A 10}$$

$$D_q\lambda_{2,3}(q) = \Big(0, 0, 1+\tan^2\vartheta, 0\Big), \tag{A 11}$$

$$D_q\lambda_4(q) = \frac{1+\tan^2(\vartheta+\mu)}{\sqrt{M^2-1}}\left(\frac{\Gamma-1}{\rho c^2}, -\frac{1}{u}, \sqrt{M^2-1}, \frac{1}{c}\left(\frac{\partial c}{\partial s}\right)_P\right), \tag{A 12}$$

so that to the above eigenpairs correspond the nonlinearity factors

$$\alpha_{1,4}(q) = \Gamma, \quad \alpha_{2,3}(q) = 0, \tag{A 13}$$

where a proper rescaling of the eigenvectors is used to eliminate the multiplicative factor in (A 10) and (A 12). Relations (A 13) reflect the role of the fundamental derivative of gasdynamics in determining the nature of the 1–field and 4–field.

REFERENCES

Alferez, N. & Touber, E. 2017 One-dimensional refraction properties of compression shocks in non-ideal gases. *J. Fluid Mech.* **814**, 185–221.

Bates, J. W. & Montgomery, D. C. 1999 Some numerical studies of exotic shock wave behavior. *Phys. Fluids* **11** (2), 462–475.

Bethe, H. A. 1942 The theory of shock waves for an arbitrary equation of state. Technical paper 545. Office Sci. Res. & Dev.

Borisov, A. A., Borisov, A. A., Kutateladze, S. S. & Nakoryakov, V. E. 1983 Rarefaction shock wave near the critical liquid-vapor point. *J. Fluid Mech.* **126**, 59–73.

Colonna, P., Guardone, A. & Nannan, N. R. 2007 Siloxanes: a new class of candidate Bethe-Zel'dovich-Thompson fluids. *Phys. Fluids* **19** (10), 086102–1–12.

Colonna, P., Guardone, A., Nannan, N. R. & Zamfirescu, C. 2008 Design of the dense gas flexible asymmetric shock tube. *J. Fluid Eng.* **130** (3), 034501–1–6.

Cramer, M. S. 1989*a* Negative nonlinearity in selected fluorocarbons. *Phys Fluids A* **1** (11), 1894–1897.

Cramer, M. S. 1989*b* Shock splitting in single-phase gases. *J. Fluid Mech.* **199**, 281–296.

Cramer, M. S. & Crickenberger, A. B. 1992 Prandtl-Meyer function for dense gases. *AIAA Journal* **30** (2), 561–564.

Cramer, M. S. & Fry, N. R. 1993 Nozzle flows of dense gases. *Phys. Fluids A* **5** (5), 1246–1259.

Cramer, M. S. & Kluwick, A. 1984 On the propagation of waves exhibiting both positive and negative nonlinearity. *J. Fluid Mech.* **142**, 9–37.

Cramer, M. S., Kluwick, A., Watson, L. T. & Pelz, W. 1986 Dissipative waves in fluids having both positive and negative nonlinearity. *J. Fluid Mech.* **169**, 323–336.

Cramer, M. S. & Sen, R. 1986 Shock formation in fluids having embedded regions of negative nonlinearity. *Phys. Fluids* **29**, 2181–2191.

Cramer, M. S. & Sen, R. 1987 Exact solutions for sonic shocks in van der Waals gases. *Phys. Fluids* **30**, 377–385.

Cramer, M. S. & Tarkenton, G. M. 1992 Transonic flows of BetheZel'dovichThompson fluids. *J. Fluid Mech.* **240**, 197–228.

Dafermos, Constantine M 2010 *Hyperbolic conservation laws in continuum physics*, , vol. 325. Springer-Verlag, Berlin,.

D'yakov, S. P. 1954 On the stability of shock waves. *Zh. Eksp. Teor. Fiz* **27** (3), 288–295.

Erpenbeck, J. J. 1962 Stability of step shocks. *Phys. Fluids* **5** (10), 1181–1187.

Fergason, S. H., Guardone, A. & Argrow, B. M. 2003 Construction and validation of a dense gas shock tube. *J. Thermophys. Heat Tr.* **17** (3), 326–333.

Fergason, S. H., Ho, T. L., Argrow, B. M. & Emanuel, G. 2001 Theory for producing a single-phase rarefaction shock wave in a shock tube. *J. Fluid Mech.* **445**, 37–54.

Fowles, G. R. 1981 Stimulated and spontaneous emission of acoustic waves from shock fronts. *Phys. Fluids* **24** (2), 220–227.

Glimm, J., Klingenberg, C., McBryan, O., Plohr, B., Sharp, D. & Yaniv, S. 1985 Front tracking and two-dimensional Riemann problems. *Advances in Applied Mathematics* **6** (3), 259–290.

Godlewski, E. & Raviart, P. A. 2013 *Numerical approximation of hyperbolic systems of conservation laws*, , vol. 118. Springer Science & Business Media.

Guardone, A. & Argrow, B. M. 2005 Nonclassical gasdynamic region of selected fluorocarbons. *Phys. Fluids* **17** (11), 116101–1–17.

Guardone, A., Vigevano, L. & Argrow, B. M. 2004 Assessment of thermodynamic models for dense gas dynamics. *Phys. Fluids* **16** (11), 3878–3887.

Guardone, A. & Vimercati, D. 2016 Exact solutions to non-classical steady nozzle flows of Bethe-Zel'dovich-Thompson fluids. *J. Fluid Mech.* **800**, 278–306.

Ivanov, A. G. & Novikov, S. A. 1961 Rarefaction shock waves in iron and steel. *Zh. Eksp. Teor. Fiz* **40** (6), 1880–1882.

Kluwick, A. 1993 Transonic nozzle flow of dense gases. *J. Fluid Mech.* **247**, 661–688.

Kluwick, A. 2001 *Handbook of Shock Waves*, chap. 3.4. Rarefaction shocks, pp. 339–411. Academic Press.

Kluwick, A. & Cox, E. A. 2018 Steady small-disturbance transonic dense gas flow past two-dimensional compression/expansion ramps. *Journal of Fluid Mechanics* **848**, 756787.

König & Thol, M. 2018 Helmholtz equation of state for tetradecamethylhexasiloxane (MD_4M). *To be submitted* .

Kontorovich, V. M. 1958 Concerning the stability of shock waves. *Soviet Phys. JETP* **6**.

Kutateladze, S. S., Nakoryakov, V. E. & Borisov, A. A. 1987 Rarefaction waves in liquid and gas-liquid media. *Ann. Rev. Fluid Mech.* **19**, 577–600.

Lambrakis, K. C. & Thompson, P. A. 1972 Existence of real fluids with a negative fundamental derivative Γ. *Phys. Fluids* **15** (5), 933–935.

Landau, L. D. & Lifshitz, E. M. 1987 *Fluid mechanics, 2nd edn.* Pergamon Press.

Lemmon, E. W., Huber, M. L. & McLinden, M. O. 2013 NIST reference database 23: reference fluid thermodynamic and transport properties–REFPROP, version 9.1. *Standard Reference Data Program* .

Mathijssen, T., Gallo, M., Casati, E., Nannan, N. R., Zamfirescu, C., Guardone, A. & Colonna, P. 2015 The flexible asymmetric shock tube (FAST): a Ludwieg tube facility for wave propagation measurements in high-temperature vapours of organic fluids. *Exp. Fluids* **56** (10), 1–12.

Menikoff, R. & Plohr, B. J. 1989 The Riemann problem for fluid flow of real materials. *Rev. Mod. Phys.* **61(1)**, 75–130.

Nannan, N. R., Guardone, A. & Colonna, P. 2014 Critical point anomalies include expansion shock waves. *Physics of Fluids* **26** (2).

Nannan, N. R., Sirianni, C., Mathijssen, T., Guardone, A. & Colonna, P. 2016 The admissibility domain of rarefaction shock waves in the near-critical vapourliquid equilibrium region of pure typical fluids. *Journal of Fluid Mechanics* **795**, 241–261.

Thompson, P. A. 1971 A fundamental derivative in gasdynamics. *Phys. Fluids* **14** (9), 1843–1849.

Thompson, P. A. 1988 *Compressilbe Fluid Dynamics*. McGraw-Hill.

Thompson, P. A., Carofano, G. C. & Kim, Y. G. 1986 Shock waves and phase changes in a large-heat-capacity fluid emerging from a tube. *J. Fluid Mech.* **166**, 57–92.

Thompson, P. A. & Lambrakis, K. C. 1973 Negative shock waves. *J. Fluid Mech.* **60**, 187–208.

Zamfirescu, C., Guardone, A. & Colonna, P. 2008 Admissibility region for rarefaction shock waves in dense gases. *J. Fluid Mech.* **599**, 363–381.

Zel'dovich, Y. B. 1946 On the possibility of rarefaction shock waves. *Zh. Eksp. Teor. Fiz.* **4**, 363–364.